Selective oxidation of methane to methanol over Au/H-MOR

Wangyang Wang[1]†, Wei Zhou[1,2]†*, Yuchen Tang[1]†, Weicheng Cao[2,3], Scott R. Docherty[2], Kang Cheng[1], Qinghong Zhang[1], Christophe Copéret[2]*, Ye Wang[1]*

[1]State Key Laboratory of Physical Chemistry of Solid Surfaces, Collaborative Innovation Center of Chemistry for Energy Materials, National Engineering Laboratory for Green Chemical Productions of Alcohols, Ethers and Esters, College of Chemistry and Chemical Engineering, Xiamen University, Xiamen 361005, China

[2]Department of Chemistry and Applied Biosciences, ETH Zürich, Vladimir-Prelog-Weg 2, CH-8093 Zürich, Switzerland

[3]Department of Chemistry, Zhejiang University, Hangzhou 310027, China

†These authors contributed equally to this work

Corresponding Authors

*e-email: weizhou@ethz.ch

*e-email: ccoperet@inorg.chem.ethz.ch

*e-email: wangye@xmu.edu.cn

Abstract

Selective oxidation of methane to methanol by molecular oxygen is a fascinating route for upgrading abundant methane resource and represents one of the most challenging reactions in chemistry due to the overwhelmingly higher reactivity of the product *versus* the reactant. Here, we report that monometallic gold nanoparticles loaded on mordenite zeolite efficiently catalyze the selective oxidation of methane to methanol by molecular oxygen in the presence of carbon monoxide in aqueous medium. The methanol productivity reaches 1300 μmol g_{cat}^{-1} h^{-1} or 280 mmol g_{Au}^{-1} h^{-1} with 75% selectivity at 150 °C, outperforming most of those reported under comparable conditions. Both hydroxyl radicals and hydroperoxide species participate in the activation and conversion of methane; the lower affinity of methanol on gold mainly accounts for higher methanol selectivity.

Methane, which is the main component of natural/shale gas and an inexpensive resource with very large reserves, can be a key feedstock in the transition of energy supplies from fossil fuels to cleaner and renewable energy, contributing to establishing a carbon-neutral society. The catalytic transformation of CH_4 into value-added liquid chemicals that are favorable for transportation and storage has attracted an increasing attention.[1] Methanol is one of the most attractive target products because of its versatility as an energy carrier or a platform molecule for the synthesis of important bulk chemicals like olefins and aromatics.[2, 3] In the current chemical industry, the conversion of CH_4 to CH_3OH relies on an energy-intensive two-step process, involving the high-temperature reforming of methane to syngas (a mixture of CO and H_2) and the high-pressure methanol synthesis. The direct conversion of CH_4 to CH_3OH, usually viewed as a "holy grail" in chemistry, would play a game-changing role in chemical utilization of CH_4. The challenge arises not only from the activation of CH_4 molecule with only inert C-H bonds but also from the selectivity control due to the overwhelmingly higher reactivity of CH_3OH compared to CH_4.

In spite of advances in CH_4 selective oxidation using a special oxidant such as oleum in homogeneous catalysis,[4] heterogeneous catalysis using molecular oxygen as an oxidant is more practically attractive but is also more challenging.[5-7] The Cu- or Fe-containing zeolite catalyst in combination with a gaseous oxidant (O_2 or N_2O) or the chemical looping approach with Cu-zeolite as a mediator has been demonstrated to be effective for gas-phase CH_4 selective oxidation, but the CH_3OH productivity is low.[8-11] The exploitation of H_2O_2 as an oxidant could enhance CH_3OH formation over several types of heterogeneous catalysts in the liquid phase,[12-17] but the reaction still suffers from limited CH_3OH productivity and CH_3OH selectivity in most cases due to the formation of other C_1 oxygenates, e.g., methyl hydroperoxide (CH_3OOH) and formic acid (HCOOH), or even CO_2. Further, the rapid decomposition of H_2O_2 leads to low efficiency of H_2O_2 usage in CH_4 selective oxidation, and the consumption of expensive H_2O_2 would hinder the practical application of the H_2O_2-based CH_4 to CH_3OH process.

The reductive activation of O_2 in the presence of a biological reductant, typically dihydronicotinamide adenine dinuleotide (NADH), is a general strategy for selective oxidation in enzymatic systems such as methane monooxygenase.[18] The exploitation of a simple

reductant such as H_2 instead of NADH for O_2 activation over a suitable catalyst could generate active species such as H_2O_2 *in situ*, accomplishing the selective oxidation of CH_4 to CH_3OH in aqueous medium.[19-21] A CH_3OH formation rate of 92 mmol g_{Au-Pd}^{-1} h^{-1} was recently achieved over a zeolite-embedded Au-Pd alloy catalyst.[20] The wasteful over-oxidation of H_2, a strong reductant, to H_2O and the risk of explosion associated with the H_2/O_2 mixture, however, need to be addressed. The use of a milder reductant carbon monoxide to activate O_2 represents an attractive alternative for the selective oxidation of CH_4 with Rh-based catalysts most commonly investigated for this reaction.[22-25] Besides CH_3OH, acetic acid could also be formed in some cases owing to the catalytic role of Rh in carbonylation in the presence of CO. [22-25] Recent studies disclosed that promoters, such as Cu^{2+} added into the aqueous solution, were required to suppress the over-oxidation of CH_3OH,[25, 26] making the system quite complicated and hard to control. The design of new types of heterogeneous catalysts and the elucidation of active species formed during the activation of O_2 by CO are needed to increase the potential of this reaction.

Here, we report our discovery that monometallic Au nanoparticles loaded on mordenite zeolite (H-MOR) with strong Brønsted acidity efficiently catalyze the direct oxidation of CH_4 to CH_3OH in aqueous medium by O_2 in the presence of CO. The CH_3OH selectivity and productivity reach 75% and 280 mmol g_{Au}^{-1} h^{-1}, respectively, without any promoters. Nuclear magnetic resonance (NMR) spectroscopy and density functional theory (DFT) calculations suggest that the weak affinity of CH_3OH on the catalyst surface is crucial to maintaining high CH_3OH selectivity.

H-MOR-supported monometallic noble metal (including Au, Rh, Pd, and Ir) catalysts with a typical nominal metal content of 0.50 wt% were prepared by an incipient wetness impregnation method, followed by H_2 reduction at 400 °C. The transmission electron microscopy (TEM) images showed that the average sizes of metal particles ranged from 3.6 to 6.5 nm (Figure S1 and S2). We observed a 2.35 Å lattice spacing for Au nanoparticles by high-resolution TEM (HRTEM), corresponding to the Au (111) facet (Figure S1B). The high-angle annual dark-field scanning transmission electron microscopy (HAADF-STEM) images and the energy dispersive X-ray (EDX) mapping revealed that the Au nanoparticles were dispersed on

the external surface of H-MOR (Figure S3). Only X-ray diffraction lines ascribed to H-MOR were observed and no diffraction lines of loaded metals appeared (Figure S4), in agreement with the high dispersion of metal nanoparticles.

The catalytic oxidation of CH_4 was performed in a batch reactor typically at 150 °C with gaseous reactants of CH_4, O_2, and CO in a molar ratio of 4/1/1 and a total pressure of 30 bar. The parent H-MOR was inactive for the conversion of CH_4, and the loading of Au, Rh, Pd, and Ir nanoparticles all catalyzed the formation of organic oxygenates from CH_4 (Table S1). The product distribution strongly depended on the identity of the noble metals (Figure 1A). The Au/H-MOR catalyst demonstrated both highest CH_3OH and lowest CO_2 selectivities; the CH_3OH selectivity reached 75% in total carbon-containing products and 94% in all organic oxygenates. Small amounts of CH_3OOH and CH_3COOH as well as trace HCOOH were detected with Au/H-MOR. In contrast, the selectivities of CH_3OH over Rh/H-MOR, Pd/H-MOR, and Ir/H-MOR were only 35%, 8.8%, and 0.9%, respectively with HCOOH formed as the major oxygenated product together with significantly more CO_2 over these catalysts. The higher selectivity of HCOOH *versus* CH_3OH was also observed for the supported Pd, Rh, and Ir catalysts reported previously.[14, 23, 26] To the best of our knowledge, this is the first report to demonstrate the high efficiency of the supported monometallic Au catalyst for the selective oxidation of CH_4 to CH_3OH by O_2.

We investigated the effect of Au loadings over the Au/H-MOR catalyst. The increase in Au loadings from 0.07 to 0.87 wt% gradually increased the average size of Au nanoparticles from 2.0 to 9.7 nm (Figure S5). The CH_3OH productivity increased significantly with the Au loading from 0.07 to 0.46 wt% and reached the maximum of about 1300 μmol g_{cat}^{-1} h^{-1} at an Au loading of 0.46 wt% (Figure 1B). CH_3OH was the major product and the selectivity of CH_3OH in organic oxygenates was maintained at ≥ 93% for all investigated Au loadings (Table S2). The CH_3OH productivity per gram of Au decreased significantly with an increase in the Au loading and the 0.07 wt% Au/H-MOR catalyst displayed the highest CH_3OH productivity per gram of Au (370 mmol g_{Au}^{-1} h^{-1}) (Figure S6). The estimated turnover frequency (TOF) of CH_3OH, i.e., the moles of CH_3OH formed per mole of surface Au sites per second, displayed a volcanic relationship with the Au particle size (Figure S7), and the Au/H-MOR with an Au particle size

of 5.9 nm showed the highest TOF, indicating that the oxidation of CH_4 to CH_3OH is a structure-sensitive reaction. The combination of CH_3OH selectivity and productivity demonstrates that the present Au/H-MOR system outperforms most of the reported catalytic systems for CH_3OH formation using O_2 in combination with CO or H_2 (Table S3). We further examined the stability of the Au/H-MOR catalyst, and no significant changes in catalytic performances were observed during the catalyst repeated uses (Figure S8). The characterizations for the used catalyst revealed no change in the crystalline structure of H-MOR and no leaching of Au to the liquid solution (Figure S9). The metallic state and the average size of Au nanoparticles were sustained after the reaction (Figure S10).

The effect of support on catalytic behaviors of the supported Au catalyst was also investigated. An Au/SiO_2 catalyst with an average Au particle size of 6.4 nm (Figure S11A) could catalyze the selective oxidation of CH_4 to CH_3OH by O_2 in the presence of CO, but the CH_3OH productivity was only 273 μmol g_{cat}^{-1} h^{-1}, about 20% of that for the Au/H-MOR catalyst (Figure 1C). Thus, the Brønsted acidity of zeolite may play a key role in the present system. Au nanoparticles with similar average particle sizes were loaded on several other typical zeolites (Figure S11B-D), and the catalytic studies revealed that all Au/zeolite catalysts showed higher CH_3OH productivity than the Au/SiO_2 catalyst. Among the supported Au catalysts investigated, the Au/H-MOR catalyst demonstrated the highest CH_3OH productivity (Figure S12 and Table S4). Previous studies revealed that H-MOR possesses the strongest Brønsted acidity and the weakest O−H bond among a series of zeolites.[27] The high activity of Au/H-MOR possibly arises from the uniquely strong Brønsted acidity of H-MOR zeolite (Figure S13). We further investigated the effect of density of Brønsted acid sites by varying the Si/Al ratio of H-MOR. The increase in the Si/Al ratio from 12.5, the typical value adopted in our work, to 20 decreased the density of Brønsted acid sites while keeping its crystalline structure (Figure S14). The average sizes of Au nanoparticle over these H-MOR samples were kept at 5.4-6.4 nm (Figure S1 and S15). The CH_3OH productivity increased significantly with the density of Brønsted acid sites in spite of slight decreases in the selectivity of CH_3OH due to the enhanced formation of CH_3OOH, CH_3COOH and CO_2 (Figure 1C and Table S5). Therefore, the Brønsted

acidity of H-MOR zeolite plays a pivotal role in the oxidation of CH_4 to CH_3OH by O_2 in the presence of CO.

The Au/H-MOR catalyst initiated CH_4 oxidation at approximately 80 °C, and CH_3OH and CH_3OOH were observed products (Figure 1D and Table S6). The formation of CH_3OH was significantly accelerated upon increasing the reaction temperature and its productivity reached as high as 1920 μmol g_{cat}^{-1} h^{-1} at 180 °C. It is noteworthy that CH_3COOH was formed considerably at 180 °C, and its selectivity and productivity increased to ~7% and ~200 μmol g_{cat}^{-1} h^{-1}. CH_3COOH is usually formed over Rh-based catalysts owing to the catalytic function of Rh site in CH_3OH carbonylation,[24, 25] thus the present result indicates that the carbonylation of the formed CH_3OH with CO could also proceed significantly at a high reaction temperature even over the supported monometallic Au catalyst. In the absence of CH_4, no oxygenated products are formed (Table 1, Entry 1). CH_3OH was formed as the major product upon introducing CH_4 and the CH_3OH productivity increased with the CH_4 pressure (Figure S16 and Table S7). These observations clearly indicate that the organic oxygenates are formed from the conversion of CH_4. The O_2 pressure was found to affect the conversion of CH_4 (Figure S17 and Table S8). At fixed CH_4 and CO pressures, a higher O_2 pressure favored the formation of CH_3OH. The CH_3OH selectivity only changed slightly at O_2 pressures ≤ 5 bar.

No products were observed in the absence of CO (Table 1, Entry 2), indicating that O_2 alone could not oxidize CH_4 at 150 °C over the Au/H-MOR catalyst. The introduction of CO induced the formation of oxygenated products as well as CO_2 (Table 1, Entry 3). The formation rates of products increased monotonically with the CO pressure, while the CH_3OH selectivity remained almost unchanged (Figure S18 and Table S9). We investigated the role of CO by performing CH_4 oxidation by O_2 in the presence of ^{13}CO instead of CO. The mass spectrum of CH_3OH formed under ^{13}CO was very close to that under normal CO (Figure S19), clearly revealing that the carbon in CH_3OH originated from CH_4 and not from CO. Further, the ^{13}C nuclear magnetic resonance (NMR) spectroscopic study for the reaction using ^{13}CO indicates that the carbon in carboxyl group of CH_3COOH originated from CO (Figure S20), confirming that the present Au/H-MOR could catalyze the carbonylation by CO to form CH_3COOH. Regarding the nature of the role of CO in accelerating CH_4 conversion, it was once proposed

that CO can assist the generation of H_2O_2 over a supported Rh catalyst by the reaction of O_2 with H_2 formed *via* water-gas shift reaction (WGS, $CO + H_2O \rightarrow CO_2 + H_2$) (*25*), whereas two other studies using Ir catalysts suggested that CO enhanced the selective oxidation of CH_4 or C_2H_6 with O_2 by maintaining the metallic state of Ir during the reaction.[26, 28] It is noteworthy that H_2O_2 was observed during the reaction of O_2, CO and H_2O over the Au/H-MOR catalyst (Table 1, Entry 1). We found that the Brønsted acidity of H-MOR favored H_2O_2 formation (Figure S21). H_2O_2 could even be detected in the presence of CH_4 and the amount of H_2O_2 showed a maximum at 120 °C (Figure S22). The decreased amount of H_2O_2 at higher temperatures might arise from the increased reactivity of CH_4. We further performed the oxidation of CH_4 using H_2O_2 as an oxidant, and the conversion of CH_4 could occur even at 50 °C, a lower temperature as compared to that for the oxidation by O_2 in the presence of CO. Similarly, CH_3OH was formed as a major product together with CH_3OOH and CO_2 but without CH_3COOH. This further supports that CH_3COOH results from carbonylation of CH_3OH with CO. The CH_3OH productivity was comparable by using (O_2 + CO) or H_2O_2 for CH_4 oxidation at the same temperature (Table 1, Entries 3 and 4, Figure 1D and Figure S23). These results suggest that the active oxygen species formed during the activation of O_2 by CO is similar to that derived by H_2O_2 over our Au/H-MOR catalyst.

Hydroxyl radicals (•OH) were assumed to be active species responsible for the oxidation of CH_4 to CH_3OH by H_2O_2 in several systems.[13, 19, 26] By using terephthalic acid as a probe molecule, which can readily react with •OH to form a product (2-hydroxyterephthalic acid) with significant fluorescence at around 420 nm,[29] we confirmed the generation of •OH radicals in the Au/H-MOR-catalyzed oxidation of CH_4 either using H_2O_2 or using O_2 in the presence of CO (Figure 2A). The electron paramagnetic resonance (EPR) spectroscopy using 5,5-dimethyl-1-pyrroline-N-oxide (DMPO) as a radical trapping agent further revealed the generation of •OH radicals during the reaction (Figure 2B).[30] We could not observe carbon-centered radicals probably because their reaction with •OH radicals was too quickly.[15] It is noteworthy that H_2 could not be detected during the oxidation of CH_4 by O_2 in the presence of CO over the Au/H-MOR catalyst. The formation of H_2 was also quite slow in the reaction of CO and H_2O, suggesting that the WGS activity of the present Au/H-MOR catalyst is negligible at 150 °C.

Thus, we speculate that H_2O_2 is not generated by the reaction between O_2 and the formed H_2 but directly from CO and O_2 in aqueous solution in the presence of our catalyst.[31] In short, the reaction involves *in situ* generation of H_2O_2 from CO, O_2, and H_2O, followed by its conversion to •OH and the subsequent oxidation of CH_4 by •OH.

The addition of an •OH scavenger, Na_2SO_3, into our system for the oxidation of CH_4 by O_2 in the presence of CO at 150 °C caused a drop in the productivity of organic oxygenates from 1380 to 507 μmol g_{cat}^{-1} h^{-1}, providing further evidence for the role of •OH in the formation of CH_3OH (Table S10). Nevertheless, the considerable remaining activity may suggest that other active species besides •OH also participates in the reaction, considering that the added scavenger is in excess and is able to quench all the •OH radicals generated during the reaction.[13] We employed *in situ* infrared (IR) spectroscopy to monitor the surface species. Two IR bands at 918 and 854 cm^{-1} were observed after the adsorption of H_2O_2 on Au/H-MOR at 50 °C (Figure S24), which could be assigned to free H_2O_2 and the O−O stretching of adsorbed peroxide species, respectively.[32, 33] The introduction of O_2, CO and H_2O gas mixture instead of H_2O_2 onto Au/H-MOR at 150 °C resulted in a broad IR band centered at 850-860 cm^{-1} (Figure 2C), indicating the formation of hydroperoxide species on the catalyst surface. Thus, we speculate that the surface hydroperoxide species might also participate in the oxidation of CH_4 to CH_3OH.

The reaction kinetics was analyzed to gain mechanistic insights into the formation of different products. The time course for the oxidation of CH_4 by O_2 in the presence of CO over the Au/H-MOR catalyst showed that CH_3OH and CH_3OOH were formed at the very initial stage with selectivities approaching 90% and 10%, respectively, and thus both were primary products (Figure 3A). The formations of CH_3OH and CH_3OOH were confirmed even after 1 min of reaction (Figure S25). Upon increasing the reaction time, the selectivity of CH_3OOH decreased and that of CH_3OH increased, indicating that CH_3OOH could be converted to CH_3OH (Figure 3A). We further compared the time course for Au/H-MOR with those for Rh/H-MOR, Ir/H-MOR, and Pd/H-MOR. CH_3OH and CH_3OOH were the primary products over all these catalysts, but the ratio of CH_3OH/CH_3OOH was the highest over the Au/H-MOR catalyst (Figure 3A and Figure S26). Furthermore, as compared to other catalysts, the Au/H-

MOR catalyst demonstrated a remarkably slower increase in the HCOOH selectivity over the time, suggesting its significantly lower ability of over-oxidation of CH_3OH. The control experiments for the oxidation of CH_3OH instead of CH_4 under equivalent conditions provided further evidence that among the catalysts investigated, the Au/H-MOR catalyst is the least active for the conversion of CH_3OH by O_2 in the presence of CO (Figure 3B).

Generally, CH_3OH can readily be oxidized into over-oxidized products by active species including •OH radicals, and this is the biggest challenge for selective oxidation of CH_4 to CH_3OH. To maintain the high selectivity of CH_3OH, a radical scavenger like Cu^{2+} is usually required to be added into the system to suppress the over-oxidation.[12, 21, 23, 26] The present work discovered that the H-MOR-supported monometallic Au catalyst offers the highest CH_3OH selectivity among a series of supported noble metal catalysts in the absence of other metal additives. The characterization with fluorescence emission spectroscopy showed that the concentration of •OH radicals during the reaction using the Au/H-MOR catalyst was not unique and was on a similar level with those using other catalysts (Figure S27). The unique CH_3OH selectivity of the Au/H-MOR catalyst suggests that besides the concentration of •OH radicals, other factors may also control the CH_3OH selectivity. The low activity of Au/H-MOR toward CH_3OH oxidation (Figure 3B) enables us to speculate that the affinity of CH_3OH on the catalyst may determine the CH_3OH selectivity, because a low affinity of CH_3OH on catalyst surfaces would mitigate its over-oxidation due to the favored desorption and the suppressed re-adsorption of CH_3OH. It is known that the relaxation time of an adsorbed molecule measured by NMR spectroscopy, described by T_1 (longitudinal relaxation time) and T_2 (transverse relaxation time), can reflect the adsorption strength of a molecule, and a higher T_1/T_2 value corresponds to a stronger interaction with the surface.[34-36] We thus measured the relaxation time for different catalysts as shown in Figure S28-S30 and Table S11. As summarized in Figure 3C, the T_1/T_2 ratio is clearly correlated to the CH_3OH selectivity. The Au/H-MOR catalyst, which has the lowest T_1/T_2 ratio and thus the lowest affinity to CH_3OH, displays the highest CH_3OH selectivity, whereas the Ir/H-MOR catalyst shows the highest T_1/T_2 ratio and the lowest CH_3OH selectivity. Therefore, our work demonstrates that the T_1/T_2 ratio is a useful

descriptor for the affinity of CH_3OH onto the catalyst surface and thus the CH_3OH selectivity during CH_4 oxidation.

We also performed computational studies to evaluate the non-dissociative adsorption energy of CH_3OH, which is closely related to its affinity, on different metal surfaces. Using a slab model, the CH_3OH molecule was adsorbed on the most representative facet, i.e., (111) facet, of different metals. The non-dissociative adsorption energy values are summarized in Figure 3D and Table S12, and the related optimized models are displayed in Figure S31-S34. The non-dissociative adsorption energy of CH_3OH on Au (111) is −0.36 eV, and its absolute value is 0.27, 0.30, and 0.63 eV lower than those on the Rh (111), Pd (111) and Ir (111) surfaces, respectively. In agreement with the NMR results, this result offers further evidence that the affinity of CH_3OH onto the Au surface is the lowest among the surfaces of metal catalysts investigated.

In conclusion, we have discovered that the H-MOR zeolite-supported monometallic Au catalyst demonstrates superior activity and selectivity in the selective oxidation of CH_4 to CH_3OH by O_2 in aqueous medium. Au nanoparticles with medium sizes and Brønsted acidity of H-MOR both play crucial roles in the formation of CH_3OH. CO is proposed to accelerate the activation of O_2 in aqueous medium to form hydroxyl radicals and hydroperoxide species responsible for the activation and conversion of CH_4. The excellent CH_3OH selectivity can be ascribed to the low affinity of CH_3OH on Au surfaces. This work opens a new avenue for the selective oxidation of CH_4 to CH_3OH as well as other important reactions, where the facilitation of product desorption is a key to selectivity.

References

1. G. Zichittella, J. Pérez-Ramírez, Status and prospects of the decentralised valorisation of natural gas into energy and energy carriers. *Chem. Soc. Rev.* **50**, 2984-3012 (2021).
2. P. Tian, Y. Wei, M. Ye, Z. Liu, Methanol to olefins (MTO): from fundamentals to commercialization. *ACS Catal.* **5**, 1922-2138 (2015).
3. I. Yarulina, A. D. Chowdhury, F. Meirer, B. M. Weckhuysen, J. Gascon, Recent trends and fundamental insights in the methanol-to-hydrocarbons process. *Nat. Catal.* **1**, 398-411 (2018).
4. R. A. Periana, D. J. Taube, S. Gamble, H. Taube, T. Satoh, H. Fujii, Platinum catalysts for the high-yield oxidation of methane to a methanol derivative. *Science* **280**, 560-564 (1998).
5. Z. Guo, B. Liu, Q. Zhang, W. Deng, Y. Wang, Y. Yang, Recent advances in heterogeneous selective oxidation catalysis for sustainable chemistry. *Chem. Soc. Rev.* **43**, 3480-3524 (2014).
6. P. Tang, Q. Zhu, Z. Wu, D. Ma, Methane activation: the past and future. *Energy Environ. Sci.* **7**, 2580-2591 (2014).
7. X. Meng, X. Cui, N. P. Rajan, L. Yu, D. Deng, X. Bao. Direct methane conversion under mild conditions by thermo-, electro-, or photocatalysis. *Chem* **5**, 2296-2325 (2019).
8. B. E. Snyder, P. Vanelderen, M. L. Bols, S. D. Hallaert, L. H. Böttger, L. Ungur, K. Pierloot, R. A. Schoonheydt, B. F. Sels, E. I. Solomon, The active site of low-temperature methane hydroxylation in iron-containing zeolites. *Nature* **536**, 317-321 (2016).
9. K. Narsimhan, K. Iyoki, K. Dinh, Y. Román-Leshkov, Catalytic oxidation of methane into methanol over copper-exchanged zeolites with oxygen at low temperature. *ACS Cent. Sci.* **2**, 424-429 (2016).
10. L. Sun, Y. Wang, C. Wang, Z. Xie, N. Guan, L. Li, Water-involved methane-selective catalytic oxidation by dioxygen over copper zeolites. *Chem* **7**, 1557-1568 (2021).
11. V. L. Sushkevich, D. Palagin, M. Ranocchiari, J. A. van Bokhoven, Selective anaerobic oxidation of methane enables direct synthesis of methanol. *Science* **356**, 523-527 (2017).
12. C. Hammond, M. M. Forde, M. H. Ab Rahim, A. Thetford, Q. He, R. L. Jenkins, N. Dimitratos, J. A. Lopez-Sanchez, N. F. Dummer, D. M. Murphy, A. F. Carley, S. H. Taylor, D. J. Willock, E. E. Stangland, J. Kang, H. Hagen, C. J. Kiely, G. J. Hutchings, Direct catalytic conversion of methane to methanol in an aqueous medium by using copper-promoted Fe-ZSM-5. *Angew. Chem. Int. Ed.* **51**, 5129-5133 (2012).

13. M. H. Ab Rahim, M. M. Forde, R. L. Jenkins, C. Hammond, Q. He, N. Dimitratos, J. A. Lopez-Sanchez, A. F. Carley, S. H. Taylor, D. J. Willock, D. M. Murphy, C. J. Kiely, G. J. Hutchings, Oxidation of methane to methanol with hydrogen peroxide using supported gold-palladium alloy nanoparticles. *Angew. Chem. Int. Ed*. **52**, 1280-1284 (2013).
14. W. Huang, S. Zhang, Y. Tang, Y. Li, L. Nguyen, Y. Li, J. Shan, D. Xiao, R. Gagne, A. I. Frenkel, F. F. Tao, Low-temperature transformation of methane to methanol on Pd_1O_4 single sites anchored on the internal surface of microporous silicate. *Angew. Chem. Int. Ed.* **55**, 13441-13445 (2016).
15. X. Cui, H. Li, Y. Wang, Y. Hu, L. Hua, H. Li, X. Han, Q. Liu, F. Yang, L. He, X. Chen, Q. Li, J. Xiao, D. Deng, X. Bao, Room-temperature methane conversion by graphene-confined single iron atoms. *Chem* **4**, 1902-1910 (2018).
16. S. Bai, F. Liu, B. Huang, F. Li, H. Lin, T. Wu, M. Sun, J. Wu, Q. Shao, Y. Xu, X. Huang, High-efficiency direct methane conversion to oxygenates on a cerium dioxide nanowires supported rhodium single-atom catalyst. *Nat. Commun.* **11**, 954 (2020).
17. P. Xie, J. Ding, Z. Yao, T. Pu, P. Zhang, Z. Huang, C. Wang, J. Zhang, N. Zecher-Freeman, H. Zong, D. Yuan, S. Deng, R. Shahbazian-Yassar, C. Wang, Oxo dicopper anchored on carbon nitride for selective oxidation of methane. *Nat. Commun.* **13**, 1375 (2022).
18. C. E. Tinberg, S. J. Lippard, Dioxygen activation in soluble methane monooxygenase. *Acc. Chem. Res.* **44**, 280-288 (2011).
19. N. Agarwal, S. J. Freakley, R. U. McVicker, S. M. Althahban, N. Dimitratos, Q. He, D. J. Morgan, R. L. Jenkins, D. J. Willock, S. H. Taylor, C. J. Kiely, G. J. Hutchings, Aqueous Au-Pd colloids catalyze selective CH_4 oxidation to CH_3OH with O_2 under mild conditions. *Science* **358**, 223-227 (2017).
20. Z. Jin, L. Wang, E. Zuidema, K. Mondal, M. Zhang, J. Zhang, C. Wang, X. Meng, H. Yang, C. Mesters, F.-S. Xiao, Hydrophobic zeolite modification for *in situ* peroxide formation in methane oxidation to methanol. *Science* **367**, 193-197 (2020).
21. B. Wu, T. Lin, M. Huang, S. Li, J. Li, X. Yu, R. Yang, F. Sun, Z. Jiang, Y. Sun, L. Zhong, Tandem catalysis for selective oxidation of methane to oxygenates using oxygen over PdCu/zeolite. *Angew. Chem. Int. Ed*. **61**, e202204116 (2022).
22. M. Lin, T. Hogan, A. Sen, A highly catalytic bimetallic system for the low-temperature selective oxidation of methane and lower alkanes with dioxygen as the oxidant. *J. Am. Chem. Soc*. **119**, 6048-6053 (1997).

23. J. Shan, M. Li, L. F. Allard, S. Lee, M. Flytzani-Stephanopoulos, Mild oxidation of methane to methanol or acetic acid on supported isolated rhodium catalysts. *Nature* **551**, 605-608 (2017).
24. Y. Tang, Y. Li, V. Fung, D. E. Jiang, W. Huang, S. Zhang, Y. Iwasawa, T. Sakata, L. Nguyen, X. Zhang, A. I. Frenkel, F. F. Tao, Single rhodium atoms anchored in micropores for efficient transformation of methane under mild conditions. *Nat. Commun.* **9**, 1231 (2018).
25. F. Gu, X. Qin, M. Li, Y. Xu, S. Hong, M. Ouyang, G. Giannakakis, S. Cao, M. Peng, J. Xie, M. Wang, D. Han, D. Xiao, X. Wang, Z. Wang, D. Ma, Selective catalytic oxidation of methane to methanol in aqueous medium over copper cations promoted by atomically dispersed rhodium on TiO_2. *Angew. Chem. Int. Ed*. **61**, e202201540 (2022).
26. M. Li, J. Shan, G. Giannakakis, M. Ouyang, S. Cao, S. Lee, L. F. Allard, M. Flytzani-Stephanopoulos, Single-step selective oxidation of methane to methanol in the aqueous phase on iridium-based catalysts. *Appl. Catal. B Environ*. **292**, 120124 (2021).
27. M. Niwa, N. Katada, New methods for the temperature-programmed desorption (TPD) of ammonia experiment for characterization of zeolite acidity: a review. *Chem. Rec.* **13**, 432-455 (2013).
28. R. Jin, M. Peng, A. Li, Y. Deng, Z. Jia, F. Huang, Y. Ling, F. Yang, H. Fu, J. Xie, X. Han, D. Xiao, Z. Jiang, H. Liu, D. Ma, Low temperature oxidation of ethane to oxygenates by oxygen over iridium-cluster catalysts. *J. Am. Chem. Soc.* **141**, 18921-18925 (2019).
29. K.-i. Ishibashi, A. Fujishima, T. Watanabe, K. Hashimoto, Detection of active oxidative species in TiO_2 photocatalysis using the fluorescence technique. *Electrochem. Commun.* **2**, 207-210 (2000).
30. P. Bilski, K. Reszka, M. Bilska, C. F. Chignell, Oxidation of the spin trap 5,5-dimethyl-1-pyrroline *N*-oxide by singlet oxygen in aqueous solution. *J. Am. Chem. Soc*. **118**, 1330-1338 (1996).
31. P. Lu, Y. Zhao, J. Dong, B.-B. Mei, X.-L. Du, Z. Jiang, Y.-M. Liu, H.-Y. He, Y.-D. Wang, X.-Z. Duan, X.-G. Zhou, Y. Cao, Direct and efficient synthesis of clean H_2O_2 from CO-assisted aqueous O_2 reduction. *ACS Catal*. **10**, 13993-14005 (2020).
32. R. Nakamura, Y. Nakato, Primary intermediates of oxygen photoevolution reaction on TiO_2 (rutile) particles, revealed by in situ FTIR absorption and photoluminescence measurements. *J. Am. Chem. Soc*. **126**, 1290-1298 (2004).

33. N. Feng, H. Lin, H. Song, L. Yang, D. Tang, F. Deng, J. Ye, Efficient and selective photocatalytic CH_4 conversion to CH_3OH with O_2 by controlling overoxidation on TiO_2. *Nat. Commun*. **12**, 4652 (2021).
34. C. D'Agostino, J. Mitchell, M. D. Mantle, L. F. Gladden, Interpretation of NMR relaxation as a tool for characterising the adsorption strength of liquids inside porous materials. *Chem. Eur. J*. **20**, 13009-13015 (2014).
35. C. D'Agostino, G. Brett, G. Divitini, C. Ducati, G. J. Hutchings, M. D. Mantle, L. F. Gladden, Increased affinity of small gold particles for glycerol oxidation over Au/TiO_2 probed by NMR relaxation methods. *ACS Catal*. **7**, 4235-4241 (2017).
36. N. Robinson, P. Bräuer, A. P. E. York, C. D'Agostino, Nuclear spin relaxation as a probe of zeolite acidity: a combined NMR and TPD investigation of pyridine in HZSM-5. *Phys. Chem. Chem. Phys*. **23**, 17752-17760 (2021).

Acknowledgments

This work was supported by the National Key Research and Development Program of Ministry of Science and Technology of China (No. 2022 YFA1504500), and the National Natural Science Foundation of China (Nos. 92145301, 22121001, 91945301, 22222206, and 21972116).

Supporting Information

Details of supplementary characterization and computations have been included in the supporting information

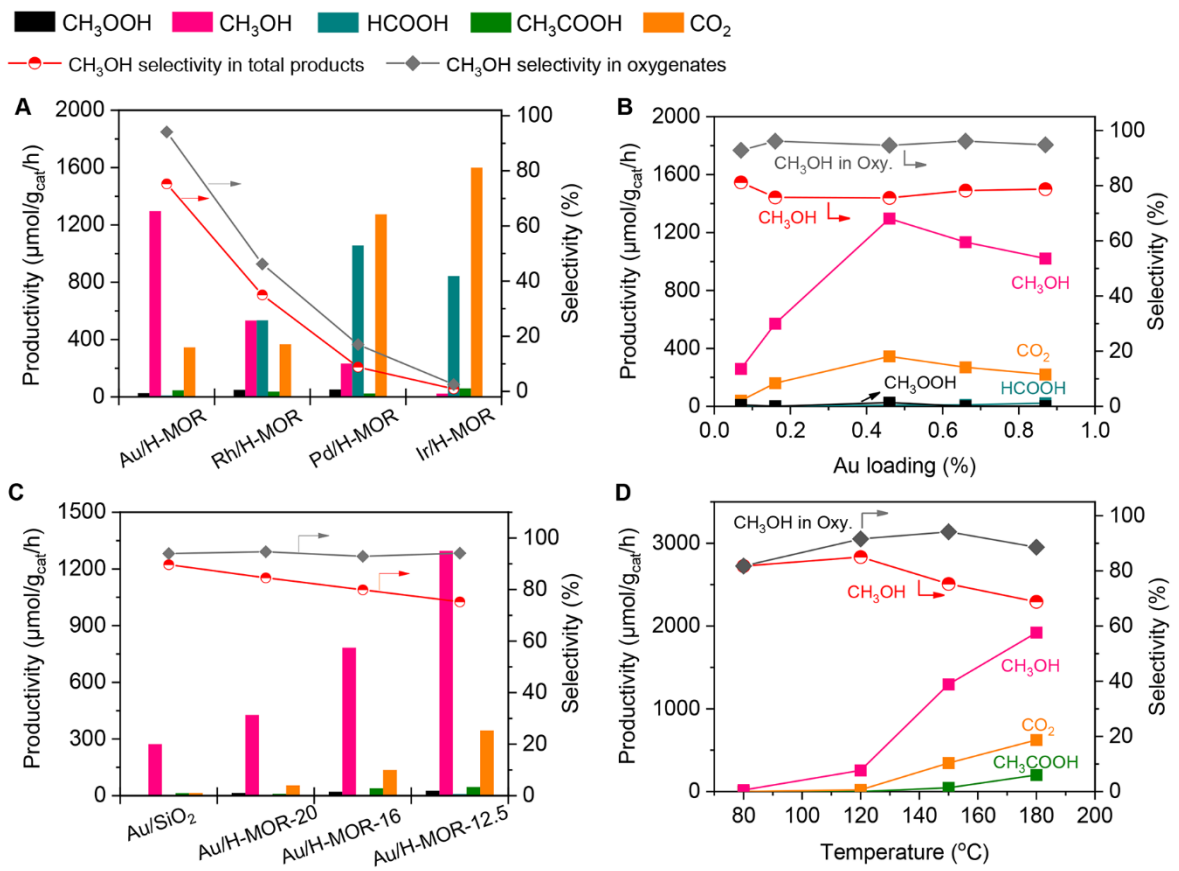

Figure 1. Catalytic performances for CH4 selective oxidation. (A) Performances of H-MOR-supported several noble metal catalysts. (B) Effect of Au loadings over the Au/H-MOR catalyst. (C) Performances of Au/SiO_2 and Au/H-MOR with different Si/Al ratios (the number after H-MOR denotes the Si/Al ratio). (D) Effect of reaction temperature. Reaction conditions: catalyst, 0.10 g; H_2O, 20 mL; total pressure, 30 bar; CH_4 pressure, 20 bar; CO pressure, 5 bar; O_2 pressure, 5 bar; reaction time, 1 h; reaction temperature, 150 °C for (A), (B), and (C).

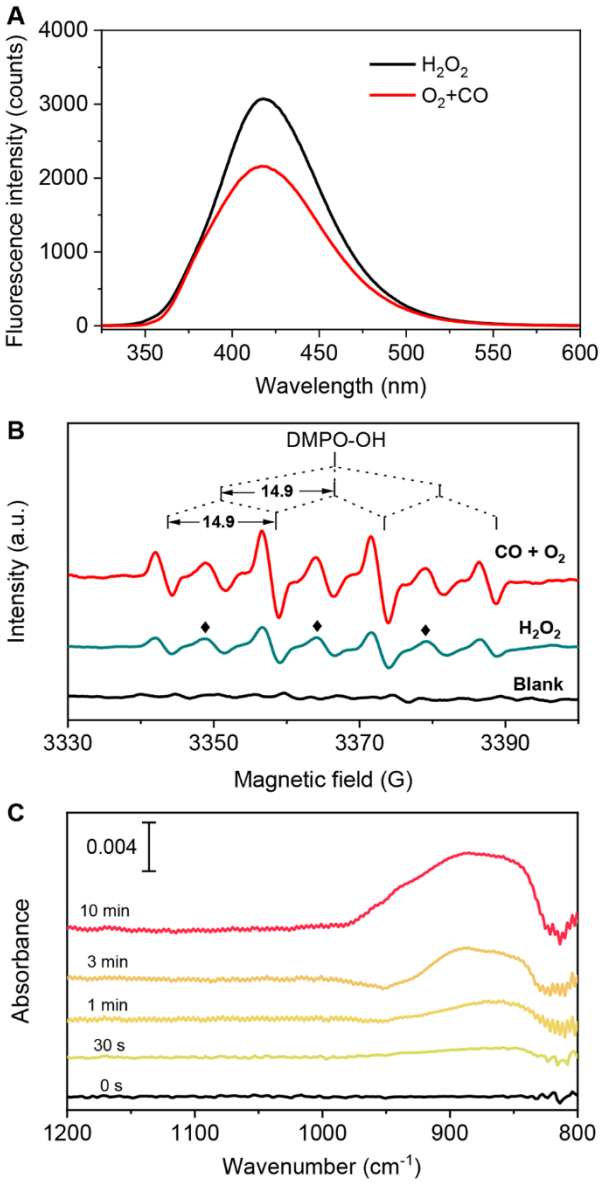

Figure 2. Characterizations of active oxygen species. (A) *In situ* fluorescence emission spectra during CH_4 oxidation by O_2 with CO or by H_2O_2 over Au/H-MOR. (B) *In situ* EPR spectra during CH_3OH oxidation by O_2 with CO or by H_2O_2 over Au/H-MOR. Signals marked by solid diamonds are attributable to the degradation of DMPO to 5,5-dimethyl-2-oxopyrroline-1-oxyl (*31*). (C) *In-situ* IR spectra of the adsorbed species on Au/H-MOR under O_2, CO and H_2O vapor.

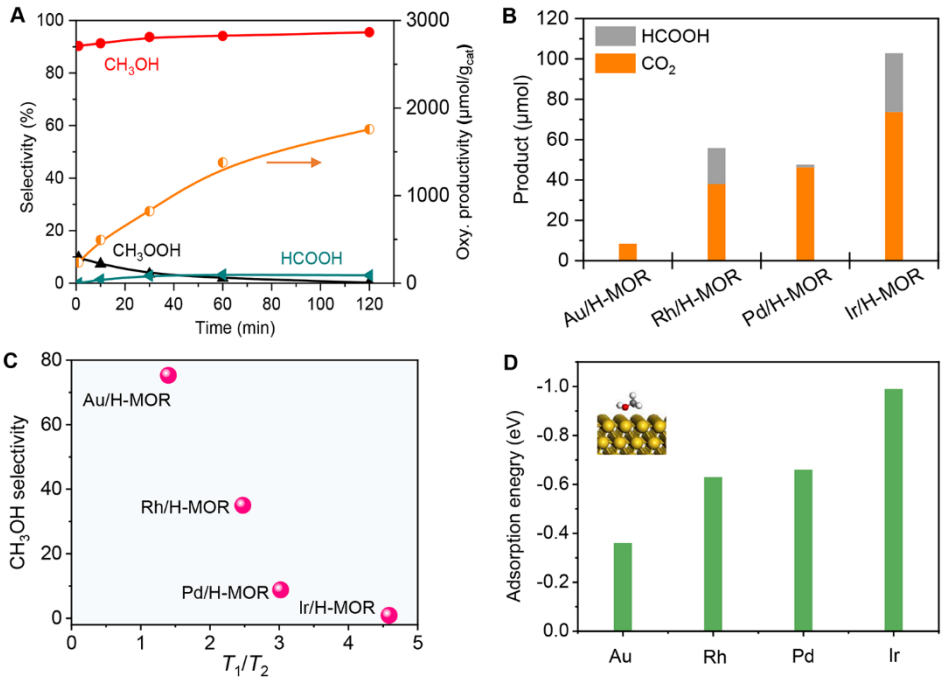

Figure 3. Relationship between CH_3OH selectivity and its affinity. (A) Changes of product selectivity and organic oxygenate productivity with reaction time during CH_4 oxidation over Au/H-MOR. Reaction conditions: catalyst, 0.10 g; H_2O, 20 mL; reaction temperature, 150 °C; total pressure, 30 bar; CH_4 pressure, 20 bar; CO pressure, 5 bar; O_2 pressure, 5 bar. (B) Amounts of HCOOH and CO_2 during the oxidation of CH_3OH. Reaction condition: catalyst, 0.10 g; H_2O, 20 mL; CH_3OH, 200 μmol; reaction temperature, 150 °C; total pressure, 30 bar; N_2 pressure, 20 bar; CO pressure, 5 bar; O_2 pressure, 5 bar; reaction time, 1 h. (C) CH_3OH selectivity during CH_4 oxidation *versus* the T_1/T_2 ratio measured by NMR. (D) Calculated non-dissociative adsorption energy of CH_3OH on noble metal surfaces. The inset represents the computation model of CH_3OH adsorbed on the Au (111) facet.

Table 1. Catalytic results for control experiments using Au/H-MOR[a]

Entry	Reactants	Amount of organic oxygenates (μmol)				CO_2 (μmol)	CH_3OH selectivity[b] (%)	CH_3OH productivity (μmol g_{cat}^{-1} h^{-1})
		CH_3OH	HCOOH	CH_3OOH	CH_3COOH			
1[c]	$CO + O_2 + N_2$	0	0	0	0	0	0	0
2	$N_2 + O_2 + CH_4$	0	0	0	0	0	0	0
3	$CO + O_2 + CH_4$	130	0.90	2.60	4.6	34.5	94.1	1300
4	$H_2O_2 + CH_4$	142	0	0	0	33.9	100	1420

[a] Reaction conditions: catalyst, 0.10 g; H_2O, 20 mL; reaction temperature, 150 °C; reaction time, 1 h; total pressure, 30 bar; CH_4 pressure, 20 bar; CO pressure, 5 bar; O_2 pressure, 5 bar.

[b] CH_3OH selectivity in all organic oxygenates.

[c] The formation of 64 μmol H_2O_2 was detected by titration of liquid products with a standard solution of $Ce(SO_4)_2$.